DOI: 10. 11835/j. issn. 2096-6717. 2021. 245

开放科学(资源服务)标识码 OSID:

# Bending wave isolation by periodic foundation with rotational oscillators

*LIU Guanchen, ZHANG Zhiwei, HUANG Jiankun, HU Yucun*

(School of Soil and Water Conservation, Beijing Forestry University, Beijing 100083, P. R. China)

**Abstract:** A periodic foundation (PF) plate with rotational oscillators was used for the bending wave isolation of high-rise buildings. Previous studies concerning the PF focused on the in-plane waves. However, seismic waves easily excite bending waves for the periodic foundation plate structure. This study broke through the limitation of plane wave research by studying the bending wave dispersion curves. The finite element method was employed to calculate the bending wave Attenuation Zones (AZs) of the PF plate by the SHELL element which can consider the influence of the plate thickness of the plate. The influences of the material and geometrical parameters on the bending wave AZs were comprehensively investigated. The effectiveness of the PF was demonstrated via a three-dimensional finite element model under incident harmonic bending-waves and seismic waves. The results show that the bending wave AZs are sensitive to the width and elastic modulus of the linkers. The bending wave AZs of the PFs were lower than 10 Hz, and the seismic isolation efficiency was greater than 60% compared to the concrete foundation, which is sufficient for it to serve as a seismic isolation foundation for high-rise buildings.

**Keywords:** periodic foundation; bending wave; attenuation zone; base isolation; numerical simulation

# 含旋转振子的周期基础对地震弯曲波的隔震作用

刘冠辰,张之伟,黄建坤,胡雨村

(北京林业大学 水土保持学院,北京 100083)

**摘　要:**提出一种含旋转振子的周期性基础(PF)板,用于高层建筑对地震弯曲波的隔震。早期对PF隔震的研究主要针对平面波,但地震波对于周期性基础板结构更易激发弯曲波。突破以往研究仅针对平面波的局限性,对弯曲波输入的频散关系进行探究;通过有限元法,利用可考虑板厚影响的SHELL单元计算PF板的弯曲波衰减域,系统研究材料参数和几何参数对弯曲波衰减域的影响;通过对三维有限元模型进行弯曲波和地震波入射的数值仿真试验,验证PF隔震的有效性。结果表明:弯曲波衰减域对连杆的宽度和弹性模量变化很敏感;在弯曲波输入下,PF的衰减域在10 Hz以下,与混凝土基础板相比,PF对弯曲波的隔震效率大于60%,能够作为高层建筑的隔震基础。

**关键词:**周期基础;弯曲波;衰减域;基础隔震;数值仿真

**中图分类号:**TU352.12　　**文献标志码:**A　　**文章编号:**2096-6717(2023)05-066-16

**Received:** 2021-06-18

**Foundation items:** National Natural Science Foundation of China (No. 31700637, 32071841)

**Author brief:** LIU Guanchen (1993- ), main research interest: periodic structure isolation, E-mail: yang67896@163.com.

HUANG Jiankun (corresponding author), PhD, associate professor, doctorial supervisor, E-mail: jiankunhuang@bjfu.edu.cn.

# 1 Introduction

Earthquake hazards are predominantly relative to infrastructure costs in repair, and some serious issues are relative to safety and fatalities and human survival. The application safety of buildings is a crucial issue for designers. Over the past four decades, innovative research and methods of seismic isolation have been proposed[1-4]. Passive, active, and semi-active control techniques have increasingly been used in civil engineering[5-6]. In recent years, the periodic structure system as a type of base isolation has been proposed with the concept of phononic crystals[7-8].

Traditional seismic isolation systems have both advantages and disadvantage. The passive isolation bearings commonly used in engineering include lead-rubber bearings, friction-type bearings, and hydraulic viscous dampers[9]. They are relatively simpler and cheaper, but they still have drawbacks. It is difficult for most passive isolation bearings to both satisfy small interstory displacement and the strong ability to block seismic energy due to the use of rubber layers[10]. An active isolation system can analyze the excitation signal to reduce vibration intensity[11]. This solves the problem of the displacement response of the isolated structure being too large under the condition of excessive seismic fortification intensity. However, the complexity of the active isolation system damages the appearance and functionality of the building. The development of new isolation materials, such as particle friction damping materials, magnetic sensitive materials, piezoelectric materials, and so on, has become a recent research trend[6]. Nonetheless, its application is greatly limited by the structural complexity and high cost. Semi-active control is a combination of active control and passive control. The stable effectiveness of weakening the seismic response of the structure is difficult to achieve, although the complexity has been reduced[12]. The semi-active and passive isolation systems are only suitable for low-rise buildings due to their low horizontal stiffness, poor durability, and large residual deformation after multi-deformations[13]. New seismic isolation systems should be developed, such as the periodic foundation (PF), which can provide enough vertical bearing capacity for high-rise buildings while simultaneously reducing the seismic waves[10,14].

The most obvious characteristic of a periodic structure (i. e. , phononic crystal) is the periodicity in the configuration and the distinctive band gap phenomenon[15]. Investigations in the field of solid-state physics have demonstrated that specific crystal arrangements can be used to manipulate the energy or patterns of acoustic (mechanical) wave energy. These materials, termed phononic crystals, can be designed to produce specific gaps in the frequency response of the structure. If the frequency contents of the wave fall within the range of the frequency bandgap of a periodic structure, the wave (i. e. , its energy) cannot propagate through the periodic structure.

As a new type of seismic isolation technique, the PF possesses a particular seismic isolation performance due to the unique dynamic characteristic of the frequency bandgap, which is also referred to as the attenuation zone (AZ). Due to the different generation mechanisms of AZs, the PFs can be divided into Bragg scattering PFs and locally resonant PFs[16]. The former has AZs whose corresponding wavelength has the same order of unit cell size as the PFs[17]. The latter possesses AZs with the unit cell size two-orders smaller than the relevant wavelength, providing a possibility to isolate seismic waves with dominant frequencies lower than 20 Hz[18-19].

This novel dynamic property has motivated researchers to fabricate periodic structures to isolate seismic waves from buildings. For instance, Jia et al. [20] proposed novel PFs to isolate seismic waves for structural protection. The feasibility and effectiveness of a one-dimensional (1D) periodic layered foundation, as well as two-dimensional (2D) and three-dimensional (3D) PFs on seismic hazard mitigation have been investigated in several comprehensive theoretical, numerical, and experimental studies[13, 21-22].

Study found that the vertical bearing capacity of the 1D PF is poor and cannot support high-rise buildings due to the rubber layers. The arrangement of the 3D PF is too complex to be manufactured in

practice. The 2D PF can meet the seismic isolation requirements of high-rise buildings both in bearing capacity and vibration reduction effectiveness. The 2D PF is effective for the incident in-plane waves, which were commonly investigated in the previous research[14,23]. However, the destructive seismic waves, which predominantly present surface waves and excite the bending vibration for a foundation plate structure, were seldom studied. The bending wave of the foundation plate is deserving of additional research to make up for the lack of existing research on this topic.

The differences between the present and previous PF research are mainly in the following aspects. Firstly, the limitation of the plane wave study was broken through, and the bending wave dispersion curves were studied. Secondly, the SHELL element rather than the plane strain element was chosen for calculating the AZ, therefore, the influence of the plate thickness was considered. Thirdly, a 3D model of a 10-storey (high-rise) building was built, which has broad applicability for modern engineering. Finally, vertical excitation was added, which can generate bending waves propagating along the horizontal plane. Therefore, the simulation is used to validate the bending wave dispersion curves and AZs. As the local site conditions did not prominently affect the reduction capacity of the AZs[13-14], the effect of local site conditions was not considered. Material damping was also neglected to emphasize the effectiveness of the AZs. If the damping was considered, the seismic reduction due to material damping and the AZ will overlap. It is difficult to distinguish the reduction between material damping and the AZ. Therefore, in the initial research of a new type of periodic structure, the material damping is usually neglected[13-14].

In this paper, a type of 2D periodic plate with rotational oscillators was used as the PF. The bending wave AZs were investigated to analyze the dynamic resistance of the overall structure under the bending wave. The rest of the paper was organized as follows. The finite element method was used to calculate the bending wave AZ of the PF in the second part. The influence of different materials and geometrical parameters on the AZs was discussed in the third section. Then, the bending wave forbidden characteristic of the PF with a ten-story superstructure (SS) is validated via numerical simulation. The mechanism of PF isolation was studied by analyzing the natural vibration characteristics of the structural systems. Finally, the conclusions were obtained.

## 2 Mathematical formulation

Modern buildings tend to be tall buildings. The ten-story frame was taken as an example. because the frame structure, which usually is set up on a raft foundation, is a common structure type for high-rise buildings. Therefore, a ten-story SS was constructed on a foundation, as presented in Fig. 1 (a). In this paper, a 2D periodic plate with rotational oscillators was used as the PF, as shown in Fig. 1 (b). For comparison, a concrete foundation (CF) of the same size was used as a type of traditional foundation, as displayed in Fig. 1(c). The periodic structure can be described by the concept of space lattice in solid-state physics because of the periodicity. As shown in Fig. 1(d), the minimal repeating elements of the periodic structure are called typical cells. The typical cell can be used to investigate the pass bands and forbidden bands of the entire periodic plate. The corresponding first Brillouin zone is presented in Fig. 1(e).

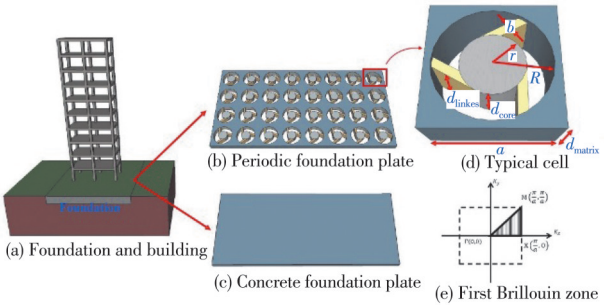


**Fig. 1 Schematic diagram of foundation with SS**

A surface wave is one of the main types of seismic waves that are trapped near the surface of the earth. For a foundation plate, the surface ground wave predominantly excites the bending wave. Therefore, the bending wave bands were investigated in the present study to analyze the structural response of the foundation plate. The basic

plate theories implemented for studying an elastic plate are the thick plate theory and the thin plate theory[24]. The thin plate theory does not apply to thicker plates, nor is it applicable to when transverse shear deformation or rotatory inertia is taken into account. In general, the oscillation's wavelength of the bending wave is less than one-fifth (or even one-tenth) of the thickness of the plate[25], therefore, the thick (Mindlin) plate theory was used to study the bending wave.

### 2.1 Governing equations

Without consideration of body force, the displacement for harmonic elastic wave propagation in a homogeneous elastic medium is represented by the following time-independent equation[26].

$$(\lambda+2\mu)\nabla(\nabla\cdot\boldsymbol{u})-\mu\nabla\times\nabla\times\boldsymbol{u}+\rho\omega^2\boldsymbol{u}=0 \quad (1)$$

where $\lambda$ and $\mu$ are Lame constants; $\rho$ is the mass density; $\boldsymbol{u}=[u, v, w]$ is the displacement vector; $\omega$ is the angular frequency; $\nabla$ is the Hamiltonian operator. When the 3D solid model is degenerated into a plate model, and the bending wave propagates along the $x$-$y$ plane (i. e., the periodic plane), and the $z$-axis is in the direction of the plate thickness, then the wave equation for the bending wave of the thick plate can be written as[25, 27-28]

$$\frac{\rho d^3}{12}\frac{\mathrm{d}^2\Theta_x}{\mathrm{d}t^2}-\frac{\partial}{\partial x}\left(D\frac{\partial\Theta_x}{\partial x}\right)-\frac{\partial}{\partial y}\left[(1-\upsilon)\frac{D}{2}\frac{\partial\Theta_x}{\partial y}\right]-\frac{\partial}{\partial x}\left(\upsilon D\frac{\partial\Theta_y}{\partial y}\right)-\frac{\partial}{\partial y}\left[(1-\upsilon)\frac{D}{2}\frac{\partial\Theta_y}{\partial x}\right]-Gkd\left(\frac{\partial w}{\partial x}-\Theta_x\right)=0 \quad (2)$$

$$\frac{\rho d^3}{12}\frac{\mathrm{d}^2\Theta_y}{\mathrm{d}t^2}-\frac{\partial}{\partial y}\left(\upsilon D\frac{\partial\Theta_x}{\partial x}\right)-\frac{\partial}{\partial x}\left[(1-\upsilon)\frac{D}{2}\frac{\partial\Theta_x}{\partial y}\right]-\frac{\partial}{\partial x}\left[(1-\upsilon)\frac{D}{2}\frac{\partial\Theta_y}{\partial x}\right]-\frac{\partial}{\partial y}\left[D\frac{\partial\Theta_y}{\partial y}\right]-Gkd\left(\frac{\partial w}{\partial y}-\Theta_y\right)=0 \quad (3)$$

$$\rho d\frac{\mathrm{d}^2 w}{\mathrm{d}t^2}-\frac{\partial}{\partial x}\left(Gkd\frac{\partial w}{\partial x}\right)-\frac{\partial}{\partial y}\left(Gkd\frac{\partial w}{\partial y}\right)+\frac{\partial}{\partial x}(Gkd\Theta_x)+\frac{\partial}{\partial y}(Gkd\Theta_y)=0 \quad (4)$$

where $\upsilon$ is the Poisson ratio; $d$ is the thickness of the plate; $t$ is time; $G$ is the shear modulus; $\Theta_x$ and $\Theta_y$ are the angle around the $x$-axis and the $y$-axis, respectively; $D=Ed^3/(1-\upsilon^2)$ is the flexural rigidity; $E$ is the elastic modulus; $k=1/1.2$ is the shear correction factor[25]; $w$ is the flexural displacement in the $z$-direction.

The ideal periodic structure is formed by the infinite repetition of the same typical cells in space, which is similar to the crystal structure. The ideal periodic structure is a lattice structure composed of typical cells distributed along the three basic translation vectors $\boldsymbol{a}_1$, $\boldsymbol{a}_2$, and $\boldsymbol{a}_3$. These three basic translation vectors are called base vectors. For this paper, a 2D periodic structure with a square lattice was studied. The lattice vector is $\boldsymbol{R}=[\boldsymbol{R}_1, \boldsymbol{R}_2]=n_1\boldsymbol{a}_1+n_2\boldsymbol{a}_2$, where $n_1$ and $n_2$ are integers. The Brillouin zone is defined by the reciprocal lattice vector $\boldsymbol{G}=m_1\boldsymbol{b}_1+m_2\boldsymbol{b}_2$, where $m_1$ and $m_2$ are integers. The corresponding reciprocal base vectors $\boldsymbol{b}_1$ and $\boldsymbol{b}_2$ can be expressed as $\boldsymbol{b}_1=(2\pi/a)$ and $\boldsymbol{b}_2=(0, 2\pi/a)$. The constant $a$ is the typical cell size.

According to the Bloch-Floquet theorem, the typical cell with periodic boundary conditions as detailed in Subsection 2.2, which can be used to represent the infinite periodic structures. The motion of the periodic domain can be expressed as follows

$$\boldsymbol{u}(\boldsymbol{r}+\boldsymbol{R})=\boldsymbol{u}(\boldsymbol{r})\cdot\mathrm{e}^{i\boldsymbol{K}\cdot\boldsymbol{R}}, \quad (5)$$

where $\boldsymbol{r}$ is the position vector; $\boldsymbol{K}=\left[K_x, K_y\right]$ is the Bloch wave vector limited to the first irreducible Brillouin zone; $\boldsymbol{u}$ is the vector of generalized nodal displacements; $i=1, 2, 3$.

Due to the geometric complexity of the typical cell, the finite element (FE) technique was employed. Condition (5) can be enforced directly in the governing Eqs. (2) - (4). In the analysis, we assume time-harmonic displacements with angular frequency $\omega$. Applying a Galerkin projection through weak form, a FE discretization of Eqs. (2)-(4) on the typical cell domain using Eq. (5) results in the standard generalized eigenvalue problem formulation

$$(\overline{\boldsymbol{K}}-\omega^2\overline{\boldsymbol{M}})\boldsymbol{u}=0, \quad (6)$$

where $\overline{\boldsymbol{K}}$ and $\overline{\boldsymbol{M}}$ are the assembled stiffness and mass matrices for the typical cell.

### 2.2 Periodic boundary conditions

According to Eq. (5), the following relationship should be satisfied for all boundary nodes of a typical cell according to the Bloch-Floquet theory.

$$\boldsymbol{u}_{\mathrm{R}}=\boldsymbol{u}_{L}\mathrm{e}^{iK_{x}a},\ \boldsymbol{u}_{\mathrm{T}}=\boldsymbol{u}_{\mathrm{B}}\mathrm{e}^{iK_{y}a},\ \boldsymbol{u}_{\mathrm{RT}}=\boldsymbol{u}_{\mathrm{LB}}\mathrm{e}^{i(K_{x}+K_{y})a} \tag{7}$$

Eq. (6) describes a finite element problem with complex boundary conditions (i. e., Eqs. (5) and (7)). Fig. 2(a) shows a typical cell with applied boundary conditions, whereas Fig. 2(b) shows the mesh of a typical cell. It is difficult for most finite element software, such as ANSYS and ABAQUS, to directly calculate models with complex boundary conditions. In this work, the two same meshed models, which respectively represent the real part and the imaginary part, were used to overcome the complex constraints. The communication between the two meshed models is expressed with a series of constraint equations

$$\begin{bmatrix}\boldsymbol{u}_{\mathrm{L}}^{\mathrm{Re}}\\ \boldsymbol{u}_{\mathrm{L}}^{\mathrm{Im}}\end{bmatrix}=\begin{bmatrix}\cos(K_{x}a) & \sin(K_{x}a)\\ -\sin(K_{x}a) & \cos(K_{x}a)\end{bmatrix}\begin{bmatrix}\boldsymbol{u}_{\mathrm{R}}^{\mathrm{Re}}\\ \boldsymbol{u}_{\mathrm{R}}^{\mathrm{Im}}\end{bmatrix}$$

$$\begin{bmatrix}\boldsymbol{u}_{\mathrm{B}}^{\mathrm{Re}}\\ \boldsymbol{u}_{\mathrm{B}}^{\mathrm{Im}}\end{bmatrix}=\begin{bmatrix}\cos(K_{y}a) & \sin(K_{y}a)\\ -\sin(K_{y}a) & \cos(K_{y}a)\end{bmatrix}\begin{bmatrix}\boldsymbol{u}_{\mathrm{T}}^{\mathrm{Re}}\\ \boldsymbol{u}_{\mathrm{T}}^{\mathrm{Im}}\end{bmatrix}$$

$$\begin{bmatrix}\boldsymbol{u}_{\mathrm{LB}}^{\mathrm{Re}}\\ \boldsymbol{u}_{\mathrm{LB}}^{\mathrm{Im}}\end{bmatrix}=\begin{bmatrix}\cos[K_{x}a+K_{y}a] & \sin[K_{x}a+K_{y}a]\\ -\sin[K_{x}a+K_{y}a] & \cos[K_{x}a+K_{y}a]\end{bmatrix}\begin{bmatrix}\boldsymbol{u}_{\mathrm{RT}}^{\mathrm{Re}}\\ \boldsymbol{u}_{\mathrm{RT}}^{\mathrm{Im}}\end{bmatrix} \tag{8}$$

where superscripts "Re" and "Im" denote real and imaginary parts of the domains.

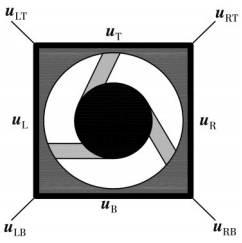


(a) Typical cell with periodic boundary condition

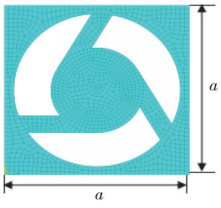


(b) meshed typical cell

**Fig. 2 Typical cell with periodic boundary condition and meshed typical cell**

In this study, ANSYS, in which SHELL181 was used, was applied to solve the eigenvalue problem (i. e., Eq. (6)) based on Eq. (8) to obtain dispersion curves of the periodic slabs. The relationship between Bloch wave vectors $\boldsymbol{K}$ and eigenfrequencies is the dispersion curve. Bloch wave vector $\boldsymbol{K}$ was swept so that the values on the boundary of the irreducible Brillouin region can be taken all over, and the dispersion curves of the intrinsic frequency spectrum with respect to Bloch wave vector $\boldsymbol{K}$ can be obtained. The frequency region in which no band exists for Bloch wave vector $\boldsymbol{K}$ in all directions is referenced as to the attenuation zone (AZ), i. e., a full gap between two bands. The typical cell is divided into quadrilateral finite elements with 6 degrees of freedom (DOFs) per node. For each node, the DOFs associated are, namely, the $z$-axial displacement and the corresponding angular deflections in the $x$ and $y$ directions.

### 2.3 Method validation

The finite element method was used to calculate the AZ of the structure in this work. The proposed method was verified by being comparing it with previously reported numerical research results. The periodic slabs in both reported studies exhibited a square configuration. In the study conducted by Qian et al. [29], the typical cell was composed of circular steel embedded in an epoxy matrix and solved via the coupled plane wave expansion and finite element method. The detailed geometrical and material parameters can be found in Ref. [29]. The corresponding dispersion curves are shown in Fig. 3 (a). Fig. 3(b) shows the dispersion curves of the periodic structure conducted by Hsu et al. [30] via the 3D plane wave expansion method. Crystalline nickel (Ni) was used as the filling material and epoxy was the matrix. The corresponding geometrical and material parameters can be found in Ref. [30]. The schematic diagrams of typical cells were shown as the inserts in Figs. 3 (a) and (b), respectively. The calculation methods of the dispersion curves in Refs. [29] and [30] were different from the present method. The theoretical dispersion curves calculated by the proposed method aligned well with previously reported methods, as presented in Fig. 3. The comparison validated the accuracy of the proposed method in calculating bending wave dispersion curves and AZs.

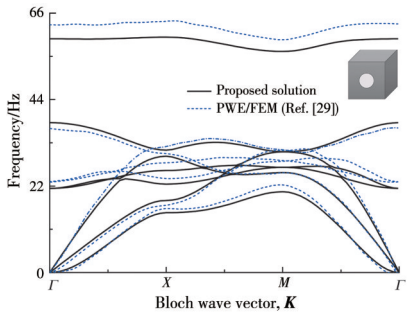


(a) The comparison between the proposed method and the method proposed by Qian et al.[29]

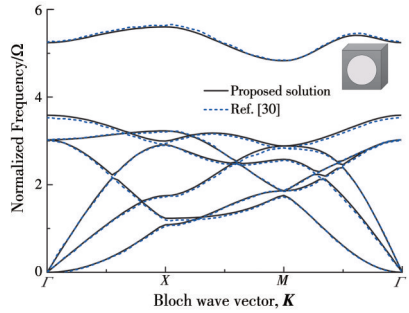


(b) The comparison between the proposed method and the method proposed by Hsu et al. [30]

**Fig. 3　Band structure of phononic crystal plate with square lattice**

## 3　Attenuation zone properties

The key and foundational research on PFs is to determine the low frequency and wide AZ, which is suitable for engineering applications. The side length of a typical cell was set as $a=1$ m. The core radius was $r=0.25$ m; the hole radius was $R=0.45$ m; the width of rubber bar was $b=0.1$ m; and the thicknesses of the matrix, rubber linkers, and core were $d_{\text{matrix}}, d_{\text{linker}}, d_{\text{core}}=0.1$ m, respectively, as shown in Fig. 1(d). The matrix of PF was made of concrete, which is usually reinforced by steel bars. It has a large vertical bearing capacity compared with the SS constructed on the 1D layered periodic structure, which has rubber layers. The rotational oscillator is a constant with three rubber linkers and a steel core, which can produce resonance and separate the band in low frequency. The AZ properties were discussed in the following. The material parameters used are listed in Table 1.

Fig. 4 shows the dispersion curves of the typical cell under the bending wave, where $\Gamma$, $X$, and $M$ are high symmetric points in the first Brillouin region. In the first part of the graph ($\Gamma \rightarrow X$), $K_x$ changes from 0 to $\pi/2$, representing the array along the $x$-direction, corresponding to $K_y=0$. In the second part ($X \rightarrow M$), $K_x=\pi/a$, $K_y=(0\text{-}\pi)/a$. In the third part ($M \rightarrow \Gamma$), $K_x=K_y=\pi/(a\text{-}0)$, changing uniformly along the diagonal direction. The bandgap range can be seen from the dispersion diagram. If the Bloch wave vector cannot be found for a specific frequency, it means the wave with this frequency cannot propagate in the structure. In this case, there is a full AZ from 3.13 Hz to 5.06 Hz, as shown in the grey area, which is consistent with the main frequency of regular seismic waves[18-19, 31-33].

**Table 1　Material parameter**

| Material | $\rho$/(kg/m$^3$) | $E$/GPa | $\upsilon$ |
|---|---|---|---|
| Concrete | 2 500 | 30 | 0.2 |
| Rubber | 1 157.3 | $3.5\times10^{-3}$ | 0.469 |
| Steel | 7 741.3 | 210 | 0.274 |
| Pb | 11 600 | 40.8 | 0.37 |
| Al | 2 716 | 70 | 0.3 |
| Cu | 8 900 | 108 | 0.34 |
| Ti | 4 500 | 110 | 0.34 |
| Fe | 7 890 | 210 | 0.3 |

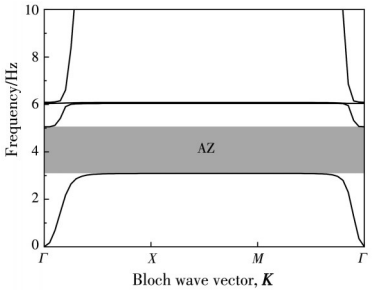


**Fig. 4　Bending-wave dispersion diagram of a typical cell**

The starting and ending frequencies and the width of the attenuation zone (WAZ) are three important parameters of the AZ. If the full AZ covered the dominant frequency range of an earthquake, the periodic foundation can isolate the seismic waves. Therefore, we should know how the parameters influence the AZ, and then obtain the optimized design parameters, especially on the first AZ. Due to its low frequency, the AZ is more valuable for seismic isolation. The characteristics of the AZs are closely related to the material parameter, component size, and structural construction[19]. Therefore, these parameters can be discussed as follows.

Fig. 5 shows the effect of the plate thickness on the AZs. When the thickness was more than $0.3a$, the starting and ending frequency and the WAZ tended to steady with the increase of the plate thickness. If the thickness was less than $0.6a$, only one AZ appeared between the first and second bands. When the thickness exceeded $0.6a$, the second AZ, which was due to the 3rd and 4th bands, appeared to remedy the shrinking of the first AZ. In general, the WAZ increased with the thickness if the plate thickness was less than $0.3a$, while the starting and ending frequency increased. If the thickness was more than $0.3a$, the WAZ was almost a constant and the starting and ending frequencies were steady. In order to ensure that the foundation has enough bearing capacity, the foundation should not be too thin and should follow the requirements of the code.

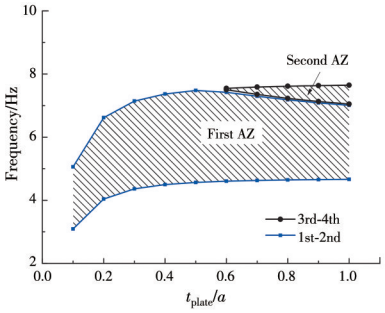


**Fig. 5 Influence of plate thickness on AZs**

Fig. 6 shows the effect of the width of rubber linker on the AZ. The starting and ending frequencies increased with the increase of width of rubber linker, and the increasing rate of the ending frequency was larger than the starting frequency. Therefore, the WAZ increased with the increase of the width of rubber linker. The rotational oscillator model can explain the starting and ending frequencies of the local resonant periodic structure. Rubber linkers and steel cores can be considered as a spring-mass oscillator. The starting frequency follows the formula $\omega = \sqrt{k/m}$. Increasing the width of rubber linker was equivalent to increasing the linker stiffness, therefore, the band frequencies increased.

Fig. 7 shows the effect of the rubber elastic modulus on the AZ. The curves show a similar trend to Fig. 6. The starting frequency can also be explained via the formula $\omega = \sqrt{k/m}$. Increasing the elastic modulus of the rubber linkers increased the value of $k$ directly, thus increasing the band

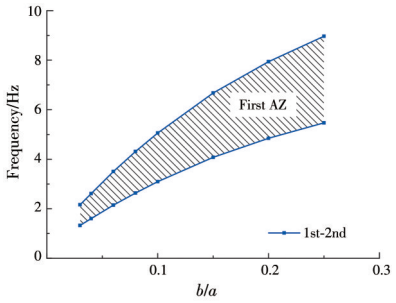


**Fig. 6 Influence of the width of rubber linker on AZs**

frequency. Therefore, the width and elastic modulus of the rubber linkers should be controlled to obtain AZs that are of lower frequency and wider.

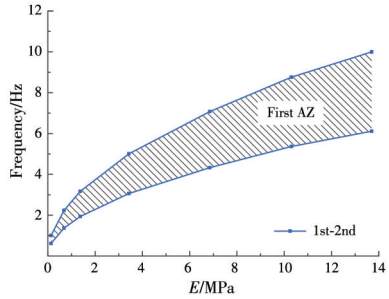


**Fig. 7 Influence of the rubber elastic modulus on AZ**

The influence of the core material on the AZ was studied by keeping the core size unchanged and only changing their material. The material parameters of the core are listed in Table 1. In Fig. 8, the curves show a contrary trend to Fig. 6 and Fig. 7. It is more useful to apply high-density material as the core to obtain an AZ with a lower frequency and a wider band. This phenomenon is of great significance to the preparation of high-density materials to cover the dominant frequency of seismic waves.

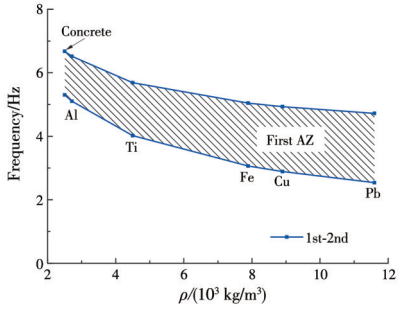


**Fig. 8 Influence of the core material on AZs**

## 4 Numerical simulation

### 4.1 Simulation model

The bending wave AZ was calculated based on an infinite medium. However, the practical structure

is finite. Therefore, a practical simulation model was established to further verify the effectiveness of PF in filtering seismic waves. The optimized parameters were used based on the above discussions and practical engineering requirements. The periodic constant of the typical cell was 2.5 m; the steel core radius was 0.625 m; the hole radius was 1.125 m; and the width of rubber linker width was 0.25 m. The thicknesses of the matrix, rubber linkers, and core were $d_{\text{matrix}}$, $d_{\text{linker}}$, $d_{\text{core}}$ =1.25, 1.15, 1.15 m, respectively. This was a gap equaling 0.05 m between the ground and rotational resonator, as well as the supersurface of plate. This configuration can make the rotational resonator move freely without touching the ground or the SS. The AZs have no obvious change because the thicknesses of the matrix, rubber linkers, and core are similar. Accordingly, only the thickness, $d_{\text{matrix}}$ = 1.25 m, was used in the calculation of dispersion curve. The material parameters for each part are shown in Table 1, except the rubber elastic modulus, which was optimized to $E_{\text{rubber}}=3.5\times10^{-2}$ GPa. In this case, it can obtain a full AZ ranging from 5.75 Hz to 9.29 Hz, which can cover the main frequency of the seismic waves in general.

The PF was composed of 4×8 typical cells. A ten-story frame structure with a story height of $h$=3 m was constructed on the foundation plate, as shown in Fig. 9(a). A concrete foundation (CF) model of the same size was established for comparison. The DOFs of the $x$- and $y$-direction for the foundation bottom were zero. This means that the foundations were supported horizontally and could move freely in the vertical direction. The core was only connected to the rubber linkers and could move freely. A vertical ($z$-direction) load with a displacement amplitude was applied on the left side of the foundation plate in order to excite the bending wave on the foundation plate. Only SOLID185 elements were used to build the simulation model, and perfect connections were considered between floors and columns as well as the foundation. The simulation model was meshed with hexahedral meshes shown as the inserts. According to the convergence requirement, the mesh size was set to less than 1/5 of the minimum wavelength[34]. Material damping was neglected in the simulation to emphasize the effectiveness of the AZs.

Key nodes that were normalized to the periodic constant on the PF were selected as the observed points (shown as the circle dots along the center line on the foundation surface in Fig. 9(a) and (b). Points $H_{N=2}$, $H_{N=4}$, $H_{N=6}$, and $H_{N=8}$ denote two, four, six, and eight periodic-constant distances, respectively, from the observed point to the incident wave. Another three points along the central axis of the SS were chosen as the vertically observed points. Points $V_{F=1}$, $V_{F=5}$, and $V_{F=10}$ denote the central node on the first floor, the fifth floor, and the top floor, as shown in Fig. 9(b). Point $H_{N=4}$ is located in the center of the ground floor. Material damping was neglected in the simulation to emphasize the effectiveness of the AZs. Due to the vertical excitation, the PF also has an effect on weakening the horizontal response. However, it is not obvious compared with the vertical attenuation effect. Therefore, only the vertical responses are shown in the following research.

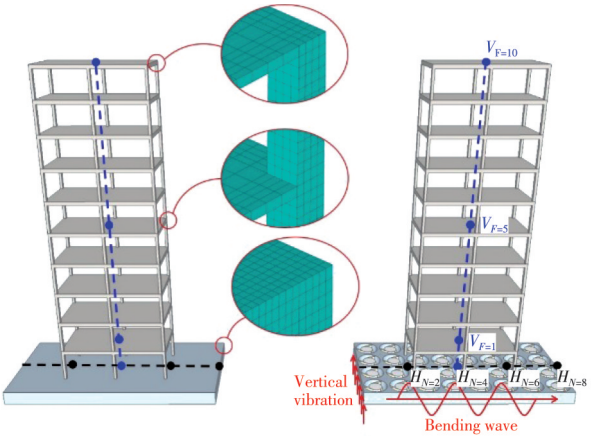


(a) CF with SS　　(b) PF with SS

**Fig. 9　CF with SS and PF with SS**

### 4.2　Responses to harmonic bending incident waves

In numerical analyses, the harmonic incident bending waves propagating along the $x$-direction were considered. The harmonic analyses were performed with a series of frequencies ($f$) to examine the dynamic responses of the PF combined with an SS. The observed frequency range of vibrations was 0-20 Hz and the step was 0.1 Hz, which were within and outside of the designed AZs. The input load function can be expressed as $P=\sin(2\pi ft)$ cm. The

governing equations and principles of the harmonic response simulation for small-amplitude excitations have previously been reported[35]. In this paper, the frequency response function (FRF) of different models was quantified by measuring the transfer function between the incident bending wave and observed output data via the formula $FRF = 20\lg(\delta_1/\delta_0)$, where $\delta_0$ and $\delta_1$ are the vertical amplitude of the incident bending wave and the vertically dynamic response, respectively.

The black solid line in Fig. 10 represents the response of the PF, while the blue dash line represents the response of the CF along the central foundation line. The shaded region in the following figures denotes the AZs. Compared to the four observation points, the attenuation effect of the PF was more obvious as the number of typical cells increased. If the periodic number reached eight, the frequency constants in the AZ were attenuated substantially. Compared with PF and CF, if the periodic number was less than four, the PF cannot appear to have added isolation capacity compared to the CF. If the periodic number continued to increase, the advantage of the AZ appeared, whereas the CF still had no definite attenuation.

The designed periodic structure owns the AZ characteristics. If the incident wave with frequencies is located on the AZ, the wave propagation will be isolated. However, if the incident wave with frequencies is outside the AZ, the amplitude of the wave will not be reduced or will even be amplified. In Fig. 10, the periodic foundation at frequencies 5 and 7 Hz is advantageous, which is located on or near the AZ (5.75 Hz to 9.29 Hz). Meanwhile, the effect is just the opposite at frequencies 12 and 14 Hz, because they are outside the AZ. The results validate the effectiveness of the AZ. The peak value within the attenuation zone (AZ) is caused by the natural structural vibration, which is explained in subsection 4.4. However, the response of the PF has an obvious attenuation in a special frequency range (i. e., AZ) compared to that of the CF. It shows that the periodic structure has a wave-filtering function in the AZ range.

Fig. 11 shows the FRF of observed points at $V_{F=1}$, $V_{F=5}$, and $V_{F=10}$ under the incident bending

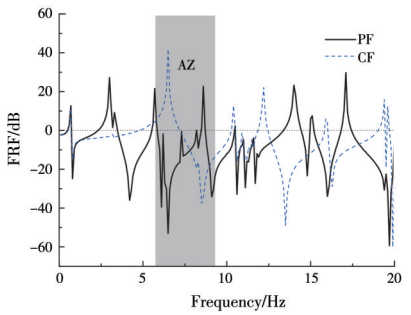


(a) $H_{N=2}$

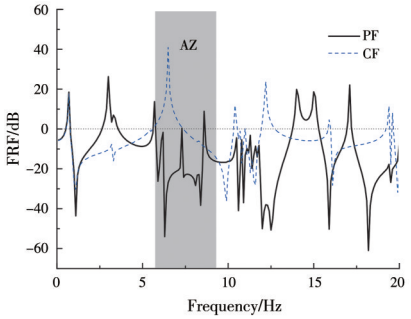


(b) $H_{N=4}$

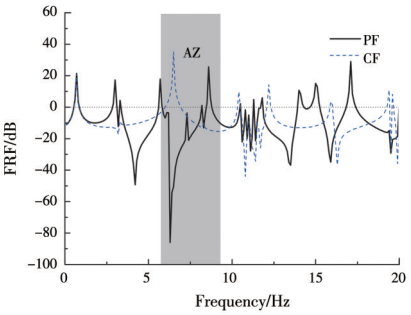


(c) $H_{N=6}$

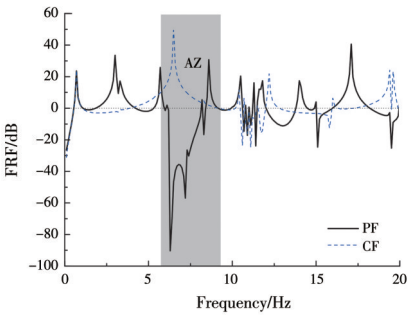


(d) $H_{N=8}$

**Fig. 10 Frequency response curves of observation points $H_{N=2}$, $H_{N=4}$, $H_{N=6}$ and $H_{N=8}$ under the bending waves**

waves. The trend of AZs was unchanged with the increase of the floor. The dynamic response of the SS on the CF was amplified as the floors were raised. However, the fluctuation response in the AZ presents obvious attenuation for the SS on the PF. It means that the PF can not only block the wave propagation along the permutation direction, but also presents effectiveness with its attachment (i. e., the

SS). The advantage of AZ shows that PF has a dramatic effect on seismic isolation of tall buildings under the bending wave incidence.

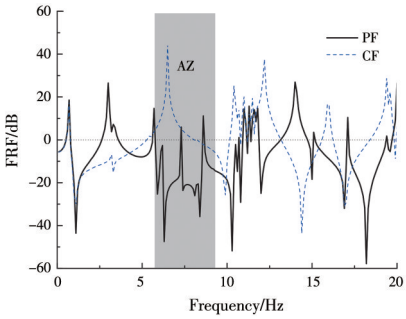


(a) $V_{F=1}$

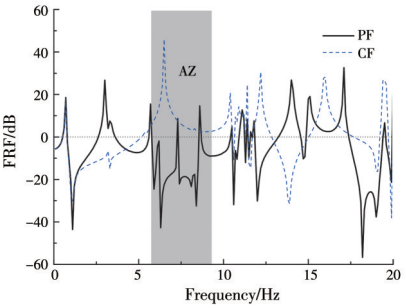


(b) $V_{F=5}$

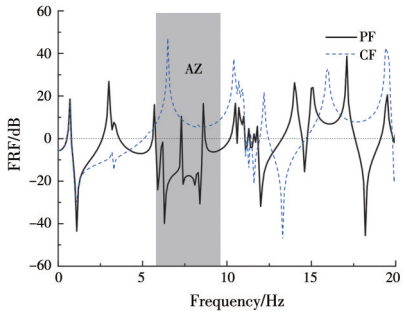


(c) $V_{F=10}$

**Fig. 11　Frequency response curves of observation points $V_{F=1}$, $V_{F=5}$, and $V_{F=10}$ under the bending waves**

### 4.3　Dynamic responses under seismic waves

This section aims to illustrate the applicability of PF under seismic waves. Two seismic waves were applied: the Oroville wave (August 1, 1975, Component 037 recorded by CDWR Station 1051, Cal.) and the Santa Felicia dam wave (San Fernando earthquake of February 9, 1971, Station No. 0284, 34.461N, 118.751W, Cal.) [31]. The horizontal incident mode of bending waves were selected to do research on the building response of seismic waves generated by distant sources. The seismic waves were integrated into the displacement load and then applied on the left side of foundation. The integration scheme used to obtain the displacement time histories was described in Ref. [31]. The dominant frequencies of Oroville and Santa Felicia waves were in the range of 0-10 Hz.

Fig. 12 shows the acceleration responses of vertical observed points $V_{F=0}$ (i. e., $H_{N=4}$), $V_{F=1}$, $V_{F=5}$, and $V_{F=10}$ in the $z$-direction under the Oroville wave ground motion. The dynamic responses of the CF achieved a peak at 1.8 s and then the energy decreased by half after 2.2 s. The acceleration of the vibration remains almost steady as the time varies for the case of PF. The steady-state acceleration of the CF was about $1.5g$, which increased to almost $2g$ with an increase in the story number. The acceleration of the SS on the PF was around $0.6g$ the entire time. The attenuation of the response peak for the PF was up to 80%-95% compared to that of CF. Meanwhile, the attenuation of the steady-state acceleration for PF was up to 60%-80% compared to that of CF. Earthquake damage was concentrated in the early instances of the wave incident. The later destructive force was relatively small. Therefore, the PF significantly reduced the destructive force of the earthquake and protected the SS.

The effectiveness of the proposed periodic foundation (PF) was determined by whether the frequencies were in the AZs. The time domain results were further analyzed in the frequency domain to investigate the effectiveness of the AZs in the special frequency domain. The frequency spectrum of point $V_{F=10}$ was analyzed by Fourier transform. The Fourier spectrum of the incident seismic wave is shown in Fig. 13(a). In Fig. 13(b), the CF has no AZ feature, therefore, the SS on the CF has no isolation effect on the AZ range under seismic waves. There is an obvious peak at 6.5 Hz, which can cause a resonant to the building. However, no waves are propagated in the AZs, as shown in Fig. 13(c). The maximum amplitude was at 3 Hz, but it was less than $0.25g$/Hz. It should be noted that an extremely small amplitude of low-frequency vibration will not cause damage to the structure. In this simulation, the PF can insulate the certain frequency fluctuation and block the specific frequency energy. This result shows the positive isolation effect of the periodic structure.

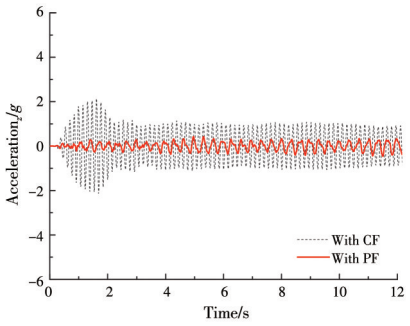


(a) $V_{F=0}$

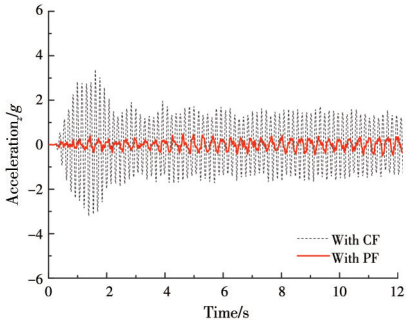


(b) $V_{F=1}$

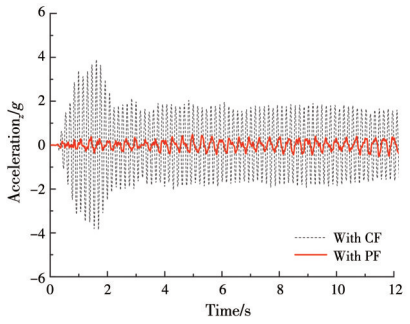


(c) $V_{F=5}$

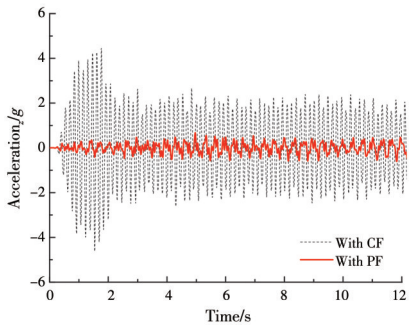


(d) $V_{F=10}$

**Fig. 12 Acceleration response of vertical observation points $V_{F=0}$ (i.e., $H_{N=4}$), $V_{F=1}$, $V_{F=5}$, and $V_{F=10}$ under the incident of the Oroville wave**

Fig. 14 shows the vertical acceleration responses of the vertical observed nodes under the incident Santa Felicia wave. The dynamic responses of higher stories become more violent compared to those of lower stories. Two acceleration peaks can be found from the curve in the case of the CF, where

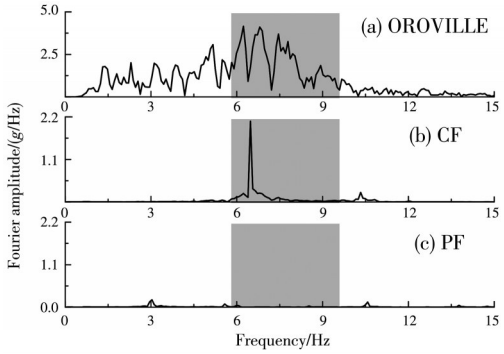


**Fig. 13 Fourier transform of acceleration response at point $V_{F=10}$ under the Oroville wave ground motion**

the main peak is near 2 s and the secondary peak is near 15 s. The rule of acceleration decrease for CF and PF under the Santa Felicia wave is similar to that of the Oroville wave. The destructive force of the earthquake was greatly reduced in the early earthquake motion and the vibration of the building was decreased for the PF.

In Fig. 15, Fourier spectrums of the point $V_{F=10}$ were analyzed. The CF has two peaks (i. e., $f$=6.18 Hz and $f$=9.23 Hz) located in the AZs. For the PF case, the PF has a small resonant at 3 Hz, and the shape of the curve is similar to that of the CF if the incident wave frequencies were outside of the AZ. However, no fluctuations can propagate within the AZ. The peak (i. e., $f$=9.23 Hz) is also attenuated significantly and the other peak (i. e., $f$=6.18 Hz) even disappeared, indicating the effectiveness of the AZs in the PF. The SS on the CF and PF has the same peak amplitude at 0.6 Hz, which corresponds to the steady-state vibrations after 15 s and proves that the two structures in Fig. 14 have the same acceleration under free vibration.

The peak reduction for PF compared with CF is 92% and 86%, respectively, in Fig. 12 and Fig. 14. That means the PF is effective in both cases of earthquakes. The PF also has the effect of isolation, when the building enters the free-vibration range, if the remaining frequencies are still in the AZs. Therefore, the PF has isolation effectiveness over the entire duration of the earthquake if the frequencies are in the AZs.

### 4.4 Bandgap generation mechanism analysis

To illustrate the generation mechanism of the AZ, the vibration modes of the structures for specific

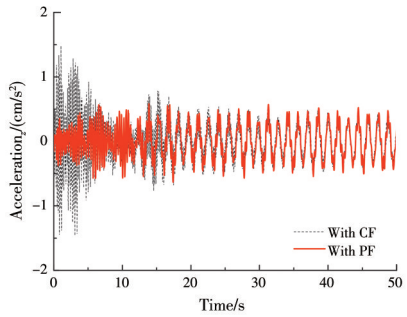


(a) $V_{F=0}$

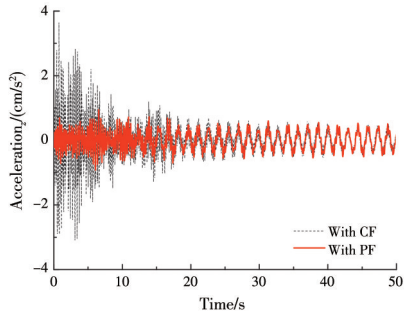


(b) $V_{F=1}$

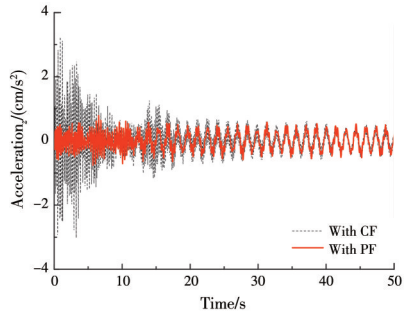


(c) $V_{F=5}$

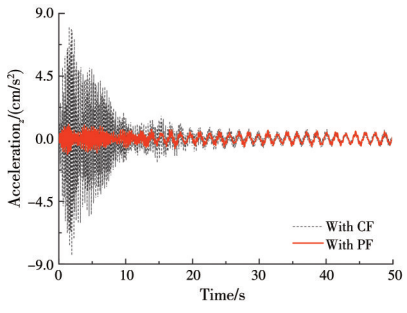


(d) $V_{F=10}$

**Fig. 14　Acceleration response of vertical observation points $V_{F=0}$ (i.e., $H_{N=4}$), $V_{F=1}$, $V_{F=5}$ and $V_{F=10}$ under the incident Santa Felicia wave**

frequencies were analyzed. Mode analysis[36] was carried out on the models including the PF, CF, and SS. The same boundary conditions mentioned above were used in the PF and CF model, and the bottoms of six columns were fixed for the SS model. The chosen modes were marked on the frequency curves, as shown in Fig. 16.

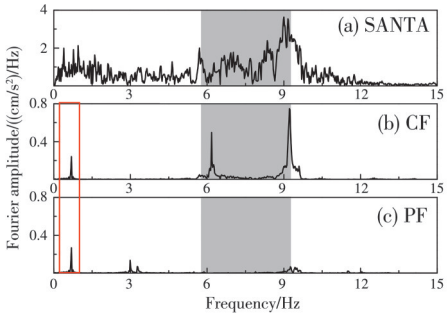


**Fig. 15　Fourier transform of acceleration response at point $V_{F=10}$ under Santa wave ground motion**

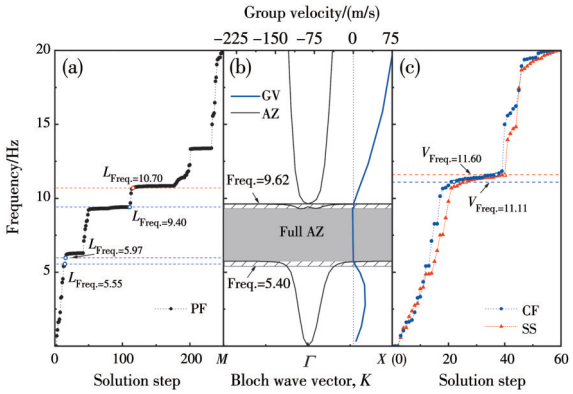


**Fig. 16　Inherent frequency analysis**

Fig. 16(a) and (c) denote the frequency curves between the solution step and mode frequency for PF, CF, and only the SS, respectively. Fig. 16(b) presents the corresponding dispersion curves of the typical cell. There are several benches on the frequency curve for PF and only one obvious bench on the frequency curves for the CF and SS. Moreover, the first two benches on the frequency curve for the PF correspond to the bands (i. e., the starting and ending frequencies) of the AZ. The frequency points $L_{\mathrm{Freq.}=5.97}$ and $L_{\mathrm{Freq.}=9.40}$ are relative to the starting and ending frequencies (5.75 Hz and 9.29 Hz) of the full AZ. In the frequency curve for the PF, the first and second bench are from 5.97 Hz to 6.28 Hz and from 9.20 Hz to 9.40 Hz, respectively. In Fig. 16(c), the frequency curve for the CF is generally consistent with that of SS. A flat segment is formed in the frequency range from 11.11 Hz ($V_{\mathrm{Freq.}=11.11}$) to 11.60 Hz ($V_{\mathrm{Freq.}=11.60}$). Compared with Figs. 16(a) and (c), there are no bending modes between points $L_{\mathrm{Freq.}=5.97}$ and $L_{\mathrm{Freq.}=9.40}$. The black dot in the AZ in Fig. 16(a) corresponds to the rotational modes, which is why it is difficult for vibrations to be excited in the AZ in Figs. 13 and

15. However, the peaks for the CF in Figs. 10 and 12 have corresponding modes, which can generate the resonance under the dominant frequency of earthquakes.

Figs. 17(a)-(c) show the vibration modes of specific frequencies $L_{\text{Freq.}=5.55}$, $L_{\text{Freq.}=5.97}$, and $L_{\text{Freq.}=9.40}$. In Figs. 17(a) and (b) the SS presents almost no motion and the wave energy makes the oscillator generate local resonance in the cavity and be consumed. The difference between Figs. 17(a) and (b) is that the entire vibration plate has a slight vibration (i. e., the plate had a sine vibration) on point $L_{\text{Freq.}=5.55}$, but has no vibration on points $L_{\text{Freq.}=5.97}$. $L_{\text{Freq.}=5.97}$ corresponds to the starting frequency but that does not mean the vibration is reduced starting from $L_{\text{Freq.}=5.97}$. The tangent line of dispersive curves denotes the group velocity (GV), which is the capacity of energy propagation[37]. The smaller the slope of tangent lines, the weaker the energy propagation. The GV is small when the frequency is close to the full AZ, as the thin blue line shows in Fig. 16(b). Therefore, vibrations would be distinctly reduced from point $L_{\text{Freq.}=5.55}$ because the slope of the tangent lines of the dispersive curves is noticeably decreased. For the same reason, the attenuation range also extends near the top of the full AZ, where it even appears as the negative GV[37]. Therefore, the actual frequency attenuation range is extended from the full AZ to the range of 5.40 Hz to 9.62 Hz at least. This is why the second peak in Fig. 15(b) can be covered by the frequency attenuation range.

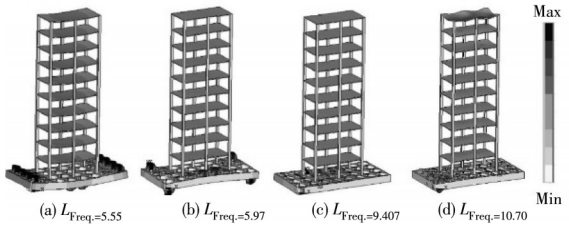


**Fig. 17 Vibration modes of structures with PF at points**

The rotational oscillators vibrate as mass-spring oscillators. The self-resonant frequencies of the model can be expressed as $\omega = \sqrt{k/m}$. The composition of forces from the rotational oscillators to the concrete matrix is nonzero and split the original dispersion curves, resulting in generation of the AZ. There are 32 oscillators in the foundation plate and each oscillator has its distinctive motion, but shows the same form in this specific frequency. Therefore, the different combinations of all oscillator vibrations formed a flat-straight segment near $f = 5.97$ and 9.40 Hz. Not all flat segments in the frequency curves of PF can generate AZs. Fig. 17(d) shows the vibration mode of the PF at point $V_{\text{Freq.}=10.70}$. The floor exhibits a bending deformation. The flat segment is attributable to the combination of different floor vibrations, indicating that the PF cannot isolate the vibration out of the AZ and energy is transferred up to the floor.

There is an approximate flat bench in the frequency curves of the CF and SS in Fig. 16(c). Vibration modes of the CF and SS are shown in Fig. 18. Different from the PF, it indicates that the energy is passed to the floor and that the vibrations are not isolated. The flat bench is caused by the combination of different floor motions near the frequencies equaling to 11.11 Hz, i. e., the local resonances of the CF and SS, which are similar in the case of the PF near $f$=10.70 Hz. However, these types of floor deformations cannot consume the wave energy. By comparing (a)-(b) and (c)-(d) in Fig. 18, the SS deformation is similar to the case with CF under the same frequency. This indicates that the CF presents no effectiveness in preventing wave propagation and wave energy absorption.

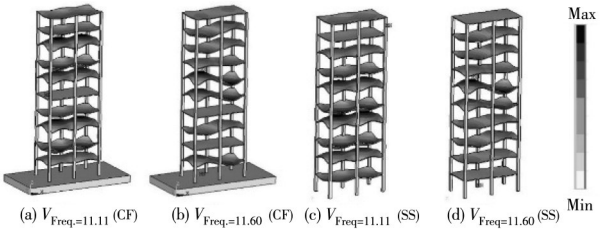


**Fig. 18 Vibration modes of structures with CF at points and SS at point**

## 5 Conclusions

The PF with rotational oscillators was studied. The influence of geometric and material parameters on the bending wave AZ was discovered. Based on these results, the performance of a finite PF with

high-rise SS was conducted. The PF isolation principle was analyzed from the perspective of the natural structural vibration. The results show that the isolation effectiveness of the PF is better than that of the CF under seismic waves. Note that the frequencies of the AZs can be designed, and the attenuation effectiveness of the foundation with SS should be verified by experiments in further research. The following conclusions can be drawn:

1) The bending wave dispersion relationships of the PF were investigated. The PF with rotational oscillators could produce bending wave AZs in the low-frequency region ($f$ <10 Hz), which can effectively reduce the propagation of seismic waves. This characteristic comprises the deficiency of the current isolation system.

2) The AZ is very sensitive to the width and elastic modulus of rubber linkers. In practical applications, it is easier to change the elastic modulus to obtain the deserved AZs and to satisfy different isolation requirements.

3) The PF exhibits effective isolation if the periodic number is up to four. The attenuation feature not only appeared at the PF, but was also effective for the attachment on the PF. The attenuation of the acceleration was more than 60% compared to the traditional CF under the Oroville wave and the Santa Felicia wave. The peak reduction for PF compared with CF is 92% and 86% for these two waves, respectively. The periodic system provides the feasibility of new base-isolation design for high-rise buildings under the vertical dynamic loadings associated with earthquakes.

## Reference


[1] TZIMAS A S, KARAVASILIS T L, BAZEOS N, et al. Extension of the hybrid force/displacement (HFD) seismic design method to 3D steel moment-resisting frame buildings [J]. Engineering Structures, 2017, 147: 486-504.

[2] VRETTOS C, BESKOS D E, TRIANTAFYLLIDIS T. Seismic pressures on rigid cantilever walls retaining elastic continuously non-homogeneous soil: An exact solution [J]. Soil Dynamics and Earthquake Engineering, 2016, 82: 142-153.

[3] CHEN X, GUAN Z G, SPENCER B F, et al. A simplified procedure for estimating nonlinear seismic demand of tall piers [J]. Engineering Structures, 2018, 174: 778-791.

[4] XIAN J H, SU C, SPENCER B F. Stochastic sensitivity analysis of energy-dissipating structures with nonlinear viscous dampers by efficient equivalent linearization technique based on explicit time-domain method [J]. Probabilistic Engineering Mechanics, 2020, 61: 103080.

[5] LI H N, WANG S Y, SONG G B, et al. Reduction of seismic forces on existing buildings with newly constructed additional stories including friction layer and dampers [J]. Journal of Sound and Vibration, 2004, 269 (3/4/5): 653-667.

[6] SONG G, SETHI V, LI H N. Vibration control of civil structures using piezoceramic smart materials: A review [J]. Engineering Structures, 2006, 28(11): 1513-1524.

[7] XU X C, BARNHART M V, LI X P, et al. Tailoring vibration suppression bands with hierarchical metamaterials containing local resonators [J]. Journal of Sound and Vibration, 2019, 442: 237-248.

[8] LIU X N, SHI Z F, MO Y L, et al. Effect of initial stress on attenuation zones of layered periodic foundations [J]. Engineering Structures, 2016, 121: 75-84.

[9] QIU C X, WANG H Y, LIU J W, et al. Experimental tests and finite element simulations of a new SMA-steel damper [J]. Smart Materials and Structures, 2020, 29 (3): 035016.

[10] SHI Z F, HUANG J K. Feasibility of reducing three-dimensional wave energy by introducing periodic foundations [J]. Soil Dynamics and Earthquake Engineering, 2013, 50: 204-212.

[11] XU L L, YU Y Y, CUI Y L. Acceleration feedback active vibration control for seismic excited building structures with actuator saturation [J]. Soil Dynamics and Earthquake Engineering, 2018, 115: 472-475.

[12] NGUYEN X B, KOMATSUZAKI T, IWATA Y, et al. Robust adaptive controller for semi-active control of uncertain structures using a magnetorheological elastomer-based isolator [J]. Journal of Sound and Vibration, 2018, 434: 192-212.

[13] WEI W, TAN P, YUAN Y, et al. Experimental and analytical investigation of the influence of compressive load on rate-dependent high-damping rubber bearings [J]. Construction and Building Materials, 2019, 200: 26-35.

[14] HUANG J K, SHI Z F, HUANG W X, et al. A periodic foundation with rotational oscillators for extremely low-frequency seismic isolation: Analysis and experimental verification [J]. Smart Materials and Structures, 2017, 26(3): 035061.

[15] VINOGRADOV E A, VESELAGO V G,

GOLOVANOV V I, et al. Dispersion characteristic of the phononic crystal and a superlens based on it [J]. Physics of Wave Phenomena, 2010, 18(1): 27-29.

[16] WANG G, LIU Y Z, WEN J H, et al. Formation mechanism of the low-frequency locally resonant band gap in the two-dimensional ternary phononic crystals [J]. Chinese Physics, 2006, 15(2): 407-411.

[17] ZONG C J, ZHANG D, DING Z D, et al. Mixed propagation modes in three Bragg propagation periods of variable chain structures [J]. IEEE Transactions on Antennas and Propagation, 2020, 68(1): 311-318.

[18] MOSCATELLI M, ARDITO R, DRIEMEIER L, et al. Band-gap structure in two- and three-dimensional cellular locally resonant materials [J]. Journal of Sound and Vibration, 2019, 454: 73-84.

[19] HUANG J K, SHI Z F, HUANG W X. Multiple band gaps of phononic crystals with quasi-Sierpinski carpet unit cells [J]. Physica B: Condensed Matter, 2017, 516: 48-54.

[20] JIA G F, SHI Z F. A new seismic isolation system and its feasibility study [J]. Earthquake Engineering and Engineering Vibration, 2010, 9(1): 75-82.

[21] WITARTO W, WANG S J, YANG C Y, et al. Three-dimensional periodic materials as seismic base isolator for nuclear infrastructure [J]. AIP Advances, 2019, 9(4): 045014.

[22] LIU X N, WANG Y H, CHEN Y C. Attenuation zones of two-dimensional periodic foundations including the effect of vertical loads [J]. Applied Sciences, 2019, 9(5): 993.

[23] CHEN Y Y, QIAN F, SCARPA F, et al. Harnessing multi-layered soil to design seismic metamaterials with ultralow frequency band gaps [J]. Materials & Design, 2019, 175: 107813.

[24] ZHU H F, SEMPERLOTTI F. Phononic thin plates with embedded acoustic black holes [J]. Physical Review B, 2015, 91(10): 104304.

[25] HALKJÆR S, SIGMUND O, JENSEN J S. Maximizing band gaps in plate structures [J]. Structural and Multidisciplinary Optimization, 2006, 32(4): 263-275.

[26] ZHAO H G, LIU Y Z, YU D L, et al. Absorptive properties of three-dimensional phononic crystal [J]. Journal of Sound and Vibration, 2007, 303(1/2): 185-194.

[27] LEISSA A W. The free vibration of rectangular plates [J]. Journal of Sound and Vibration, 1973, 31(3): 257-293.

[28] EASON G. Wave motion in elastic solids 1975 [J]. Journal of Sound and Vibration, 1975, 43(4): 721-722.

[29] QIAN D H, SHI Z Y. Using PWE/FE method to calculate the band structures of the semi-infinite PCs: Periodic in x-y plane and finite in z-direction [J]. Archives of Acoustics, 2017, 42(4): 735-742.

[30] HSU J C, WU T T. 4G-1 A fast algorithm for calculating band structures in two-dimensional phononic-crystal plates [C]//2006 IEEE Ultrasonics Symposium. October 2-6, 2006, Vancouver, BC, Canada. IEEE, 2006: 665-668.

[31] PEER. Peer Ground Motion Database [DB/OL]. http://peer.berkeley.edu/.

[32] BRILLOUIN L. Wave propagation in periodic structures [M]. Dover, 1946.

[33] HSU J C, WU T T. Bleustein-Gulyaev-Shimizu surface acoustic waves in two-dimensional piezoelectric phononic crystals [J]. IEEE Transactions on Ultrasonics, Ferroelectrics, and Frequency Control, 2006, 53(6): 1169-1176.

[34] HUANG J K, LIU W, SHI Z F. Surface-wave attenuation zone of layered periodic structures and feasible application in ground vibration reduction [J]. Construction and Building Materials, 2017, 141: 1-11.

[35] XU Y L, CAO L Y, YANG Z C. Deflecting incident flexural waves by nonresonant single-phase meta-slab with subunits of graded thicknesses [J]. Journal of Sound and Vibration, 2019, 454: 51-62.

[36] YU Y C, ZHANG S J, LI H, et al. Modal and harmonic response analysis of key components of ditch device based on ANSYS [J]. Procedia Engineering, 2017, 174: 956-964.

[37] HUANG J K, RUZZENE M, CHEN S B. Analysis of in-plane wave propagation in periodic structures with Sierpinski-carpet unit cells [J]. Journal of Sound and Vibration, 2017, 395: 127-141.

(编辑 黄廷)